Simulation Standard

Engineered Excellence

A Journal for Process and Device Engineers

Generally Applicable Degradation Model for Silicon MOS Devices

Introduction

The main cause of operational degradation in MOS devices is believed to be due to the buildup of charge at the Silicon-Oxide interface. This leads to reduced saturation currents and threshold voltage shifts in MOSFET devices. Physics-based models of the degradation process typically consider the breaking of Si-H bonds (depassivation) at the Silicon-Oxide interface to be the main cause of the operational degradation. A new general model of Si-H bond breaking has recently been included in Atlas, adding to the Silvaco TCAD portfolio of degradation models[1].

This article presents the theory of the new model, and describes its implementation in Atlas. The model is then applied to a simple MOSFET to illustrate the features of the model. Finally it is applied to model a realistic MOSFET for which experimental degradation data are available. It is able to simulate reasonably well the unusual behavior of the degradation as a function of stressing time.

General Framework Model

The model is based on a study of Si-H trap dynamics in which three bond breaking mechanisms are considered[2]. The first mechanism occurs at high electric field, which distorts the bond and reduces the amount of thermal energy needed to break the bond. The second mechanism involves a high energy (hot) carrier breaking the bond with a single interaction, and the third involves many lower energy (cold) carriers exciting a vibrational mode to higher and higher energies until the bond breaks. These two different carrier mediated processes are necessary in order to explain some aspects of Hot Carrier Degradation [3]. Along with that work, we refer to the hot carrier process as single-particle (SP) and the cold carrier process as multi-particle (MP). First we describe the single-particle process. The time evolution of the interface charge is assumed to be of the form

$$N(\mathbf{r},t) = {}^{sp}_{it}N \quad (1.0 - \exp(-t\,K_f^e(SP)(\mathbf{r}))) \qquad [1]$$

for electrons, where N(**r**,t) is negative interface charge density, and

$$P(\mathbf{r},t) = N_d^{sp}\ (1.0 - \exp(-t\,K_f^h(SP)(\mathbf{r}))) \qquad [2]$$

for holes, where P(**r**,t) is positive interface charge density. The quantities N_a^{sp} and N_d^{sp} represent the saturated values of negative and positive interface charge density associated with the SP process, and the time is t in seconds. The reaction rate for this process at position r is given by

$$K_f^{e,h}(SP)(\mathbf{r}) = \int_{E_{sp}}^{\infty} f(E,\mathbf{r})g(E)u_g(E)\sigma_{sp}^{e,h}(E,E_{sp})dE \qquad [3]$$

where $f(E, \mathbf{r})$ is the anti-symmetric part of the carrier distribution function, $g(E)$ is the density of states and u_g is the group velocity. For electrons, the function $\sigma_{sp}^e(E, E_{sp})$ is defined for $E \geq E_{sp}$, where

$$\sigma_{sp}^e(E,E_{sp}) = \sigma_{sp,0}^e \left(\frac{E - E_{sp}^e}{K_bT}\right)^{M_{sp}^e} \qquad [4]$$

where the Boltzmann energy K_bT acts as an energy scale. This is known as a soft-threshold, as introduced by Keldysh in the context of impact ionization rate calculations. Therefore only electrons with an energy of more than E_{sp} contribute to this integral. Analagously, the function is defined for holes as

$$\sigma_{sp}^h(E,E_{sp}) = \sigma_{sp,0}^h \left(\frac{E - E_{sp}^h}{K_bT}\right)^{M_{sp}^h} \qquad [5]$$

Continued on page 2 ...

INSIDE

Simulations of Deep-Level Transient Spectroscopy for 4H-SiC 8

Hints, Tips and Solutions 11

Equation [3] is often referred to as an acceleration integral in the literature, although its units are s^{-1}.

The MP process involves gradual excitation of the bending vibrational quantum states of the bond by less energetic carriers, followed by a thermal excitation from the highest bound state to the transport state of the Hydrogen. This thermal emission occurs over a barrier of height E_{emi} eV, with an attempt frequency of ν_{emi} Hz, giving an emission rate of

$$P_{emi} = \nu_{emi} \exp(-E_{emi}/K_b T) \quad [6]$$

where T is the lattice temperature. There is also the reverse process for repassivation of the bond, where the hydrogen overcomes a barrier of height E_{pass} to become bonded again. The overall repassivation rate is

$$P_{pass} = \nu_{pass} \exp(-E_{pass}/K_b T) \quad [7]$$

The excitation of the bond by numerous cold carriers can be described by a set of coupled differential equations describing the occupation density of each level [2]. Entering these equations as parameters are P_u and P_d which are the probabilities of transition to the next higher vibrational state and the next lower vibrational state respectively. These are modelled by the expressions

$$P_u = \nu_{phon} \exp(-\hbar\omega/K_b T) + K_f^{e,h}(MP)(\mathbf{r}) \quad [8]$$

and

$$P_d = \nu_{phon} + K_f^{e,h}(MP)(\mathbf{r}) \quad [9]$$

where ν_{phon} is an attempt frequency and $\hbar\omega$ is the vibrational mode energy. The acceleration integral is

$$K_f^{e,h}(MP)(\mathbf{r}) = \int_{E_{mp}}^{\infty} f(E,\mathbf{r}) g(E) u_g(E) \sigma_{mp}^{e,h}(E,E_{mp}) dE \quad [10]$$

where $f(E,\mathbf{r})$ is the anti-symmetric part of the carrier distribution function. The cross-section $\sigma_{mp}^{e,h}(E,E_{mp})$ is given by the expression

$$\sigma_{mp}^{e,h}(E,E_{mp}) = \sigma_{mp,0}^{e,h} \left(\frac{E - E_{mp}^{e,h}}{K_b T}\right)^{M_{mp}^{e,h}} \quad [11]$$

Because these processes depend on cold carriers, the threshold energies are less than the threshold energies in the SP process. After some mathematical manipulation and simplification, the density of traps created by the MP process is given by

$$N(\mathbf{r},t) = N_a^{mp}\left[\frac{P_{emi}}{P_{pass}}\left(\frac{P_u}{P_d}\right)^{Nl}(1.0 - \exp(-t\,P_{emi}))\right]^{1/2} \quad [12]$$

for electrons, where N(**r**,t) is negative interface charge density, and

$$P(\mathbf{r},t) = N_d^{mp}\left[\frac{P_{emi}}{P_{pass}}\left(\frac{P_u}{P_d}\right)^{Nl}(1.0 - \exp(-t\,P_{emi}))\right]^{1/2} \quad [13]$$

for holes, where P(**r**, t) is positive interface charge density. *Nl* is the number of bending mode vibrational levels in the Si-H bond. Analysis of equations (12) and (13) shows that the time evolution depends only on the emission rate. The saturation level depends on the unpassivated bond densities N_a^{mp} and N_d^{mp}, ratio of depassivation rate to passivation rate and the ratio of P_u to P_d, raised to the power of Nl. This last ratio will be very small in the absence of a significant acceleration integral, as it will be a Boltzmann factor with energy of approximately the binding energy of the ground state. From equations (8) and (9) it is seen that if $K_f^{e,h}(MP)(\mathbf{r})$ is greater than the attempt frequency, the ratio of P_u to P_d is approximately one. The spatial distribution of traps depends, therefore, in a very non-linear manner on the acceleration integral.

The third component of the general framework model is a field-enhanced thermal degradation, which is modelled as

$$P_{therm} = K_{therm} \exp(-E_b/K_b T) \quad [14]$$

where K_{therm} is an attempt frequency and E_b is the Field dependent Si-H bond energy.

P_{therm} has the same time dependence as the SP process and so it is simply added to $K_f^{e,h}(SP)(\mathbf{r})$ in the calculation of defects after stressing time t.

Many of the model parameters can be set on the DEGRADATION, MATERIAL or MODELS statements. For example NTA.SP, NTA.MP, NTD.SP and NTD.MP on the DEGRADATION statement specify N_a^{sp}, N_a^{mp}, N_d^{sp}, N_d^{mp} respectively

Calculation of the Carrier Distribution Function

Equations (3) and (10) require the anti-symmetric part of the carrier distribution function. The capability to solve the Boltzmann Transport Equation (BTE) for the zeroth and first order terms in a Spherical Harmonic expansion of the carrier distribution function has recently been added to Atlas. The first order term is anti-symmetric and is used in equations (3) and (10). In a similar model Starkov et al [3] used Monte Carlo simulations to estimate the carrier distribution function. Reggiani et al [4] used an analytical formulation for the carrier distribution function, with parameters derived from the Spherical harmonic expansion solution to the Boltzmann transport equation. This approximation was made to improve calculation speed. The Atlas implementation of the BTE solver is sufficiently rapid that a further approximation

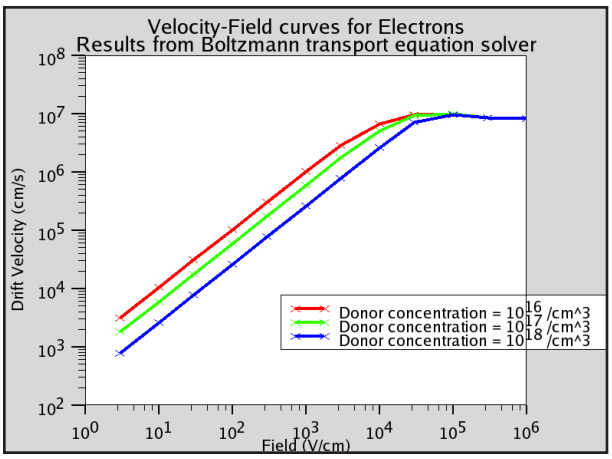
Velocity-Field curves for Electrons
Results from Boltzmann transport equation solver
Drift Velocity (cm/s)
Field (V/cm)
Donor concentration = 10^16 /cm^3
Donor concentration = 10^17 /cm^3
Donor concentration = 10^18 /cm^3

Figure 1. Homogeneous velocity field curves for electrons.

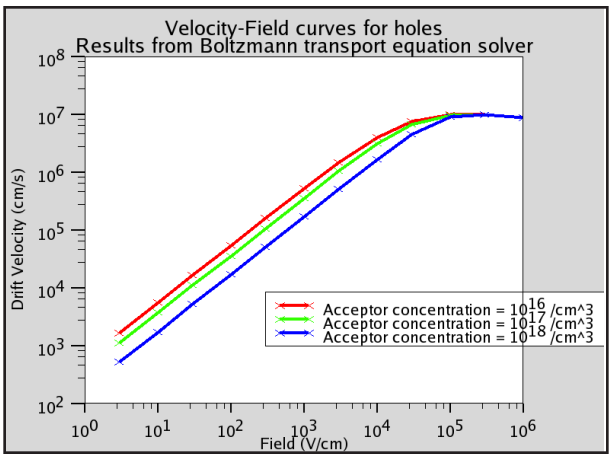
Velocity-Field curves for holes
Results from Boltzmann transport equation solver
Drift Velocity (cm/s)
Field (V/cm)
Acceptor concentration = 10^16 /cm^3
Acceptor concentration = 10^17 /cm^3
Acceptor concentration = 10^18 /cm^3

Figure 2. Homogeneous velocity field curves for holes.

of the carrier distribution function is not necessary. The BTE solver is based on the formulation of Ventura et al [5]. The equation for the zeroth order expansion, f_o, of the carrier distribution function is

$$\frac{\partial}{\partial x}\left(g(E)\tau(E)u_x^2(E)\frac{\partial f_o}{\partial x}\right) + \frac{\partial}{\partial y}\left(g(E)\tau(E)u_y^2(E)\frac{\partial f_o}{\partial y}\right)$$
$$+3\,g(E)c_{op}\,[g(E+\hbar\omega)(N_{op}^{+}f_o(E+\hbar\omega)-N_{op}f_o(E)) \qquad (15)$$
$$-g(E-\hbar\omega)\,(N_{op}^{+}f_o(E)-N_{op}f_o(E-\hbar\omega))]=0$$

where E is energy in eV, $g(E)$ is the density of states in $m^{-3}e\upsilon^{-1}$, F is field in V/m, $\tau(E)$ is a scattering lifetime in seconds, u_g is the group velocity in m/s, c_{op} is optical phonon scattering coefficient in m^3J/s, N_{op} is the optical phonon occupation number and the optical phonon energy is $\hbar\omega$ in eV. N_{op}^{+} is the optical phonon occupation number plus one, simplified as follows

$$N_{op}^{+} = N_{op} + 1 = exp(q\hbar\omega/K_bT_l)N_{op} \qquad (16)$$

where K_b is Boltzmanns constant and Tl is the lattice temperature. The first order expansion, f_1, is then obtained from

$$f_1 = q\tau(E)u_g(E)F\frac{\partial f_o}{\partial E} \qquad (17)$$

The lifetime τ(E) is derived from the carrier scattering mechanisms. Scattering mechanisms which are included by default are optical phonon scattering, acoustic phonon scattering and ionized impurity scattering. Impact ionization scattering can also be included if required. Quantities such as carrier density, drift velocity and energy can be calculated from the carrier distribution functions. For example, the drift velocities as a function of homogeneous field are shown in Figure 1 for electrons and Figure 2 for holes. Results are shown for three different values of dopant concentration.

To initialize Atlas for solving the BTE, the flags BTE.PP.E for electrons and BTE.PP.H for holes must be set on the MODELS statement. After the BTE has been solved for a specific bias set, Atlas includes the acceleration integrals when it saves the structure to file. See the Atlas manual[1] for more details on the BTE solver.

Implementation of the General Framework Model

An Atlas device is biased to the stressing configuration using the drift-diffusion or energy-balance models. A SOLVE statement with the flags DEVDEG.GF.E for electrons and DEVDEG.GF.H for holes will solve the Boltzmann transport equation. Up to 10 degradation times can be simulated using the parameters TD1 .. TD10 on the SOLVE statement. The interface charge densities are calculated using equations (1), (2), (12) and (13) for each requested degradation time, and the results are written to a structure file. For example, the Atlas statement

```
SOLVE DEVDEG.GF.E TD1=1.0e-2
TD2=1.0e-1 TD3=1.0 TD4=10.0 TD5=1.0e2
OUTFILE=simstd.str
```

will result in files

```
simstd_1.00e-02s.str
simstd_1.00e-01s.str
simstd_1.00e+00s.str
simstd_1.00e+01s.str
simstd_1.00e+02s.str
```

being written out, each having an interface charge density corresponding to the simulated degradation time.

Example: Simple MOSFET

The first example is for the MOSFET structure shown in Figure 3. Each of the three different degradation models

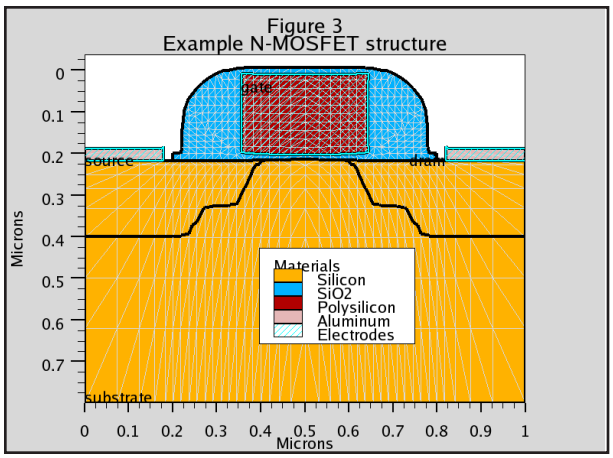

Figure 3. Example structure.

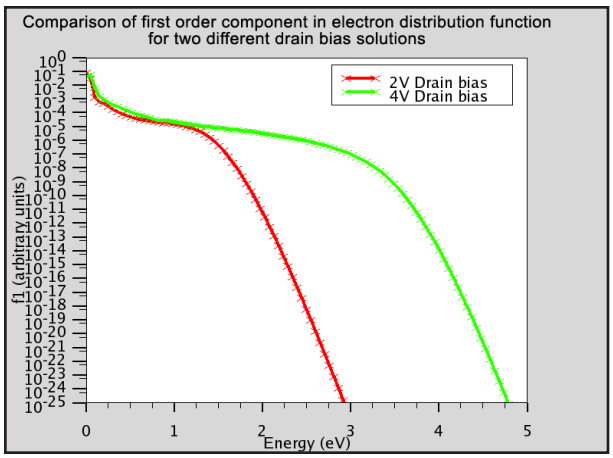
Comparison of first order component in electron distribution function
for two different drain bias solutions
2V Drain bias
4V Drain bias
f1 (arbitrary units)
Energy (eV)

Figure 6. First order component of electron distribution function.

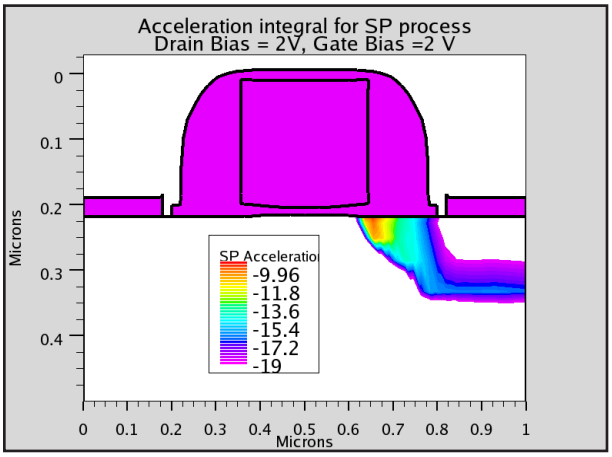

Figure 4. SP Acceleration integral at 2V drain bias (logarithmic scale).

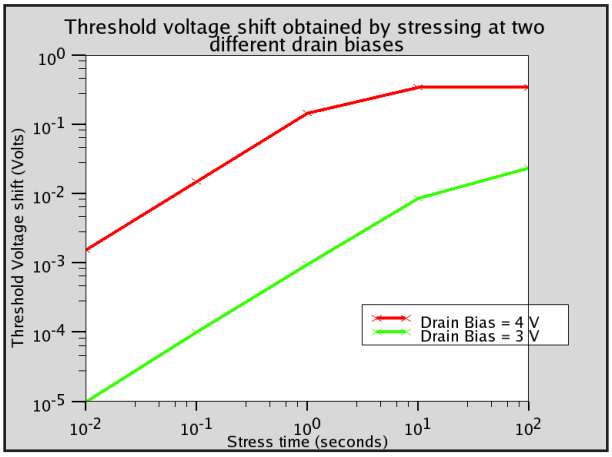
Threshold voltage shift obtained by stressing at two
different drain biases
Drain Bias = 4 V
Drain Bias = 3 V
Threshold Voltage shift (Volts)
Stress time (seconds)

Figure 7. Threshold Voltage shifts due to SP process as a function of stressing time.

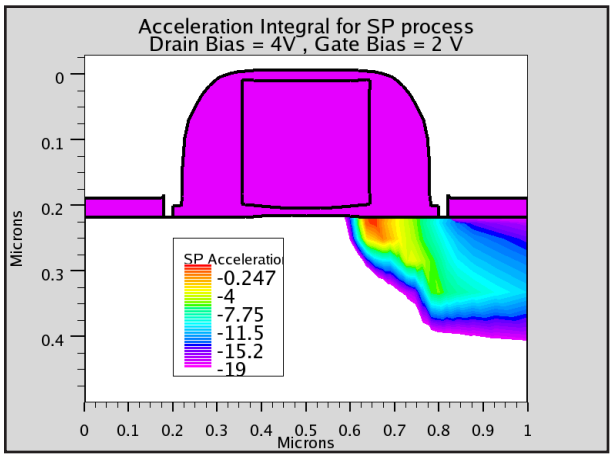

Figure 5. SP Acceleration integral at 4V drain bias (logarithmic scale).

are looked at in turn for the case of electrons in this device. The MP Keldysh cross-section $\sigma^{e}_{mp,0}$ was set to zero and the SP Keldysh cross-section was set to be 1.0×10^{-22} cm^2, with a threshold energy of 2.2 eV. The saturated dangling bond density N^{a}_{sp} was set to 4×10^{12} cm^{-2}. With a gate bias of 2 V, a BTE solution was obtained at a drain voltage of 2 V and also at a drain Voltage of 4 V. The acceleration integral for the SP process is shown in Figure 4 for 2V Drain bias and Figure 5 for 4V Drain bias. At 4V drain bias it is many orders of magnitude larger than at 2V drain bias. In Figure 6 the first order component of the electron distribution function is plotted, at the node where the SP acceleration integral is a maximum. The electron distribution function at 4V drain bias is much larger at higher energies than the equivalent distribution at 2V drain bias. The energy threshold in the calculation of acceleration integral is 2.2 eV, and clearly the electron distribution function at 4V drain bias is much larger above this energy.

The simulation was performed with degradation times of 10 milliseconds, 100 milliseconds, 1 second, 10 seconds and 100 seconds. The threshold Voltage after each simulation time was calculated from the Gate bias required to achieve a specified drain current, and the threshold Voltage shifts calculated. At 2V drain bias there was negligible threshold voltage shift, and so the calculation was performed with drain biases of 3V and 4V, with the resulting shifts being shown in Figure 7.

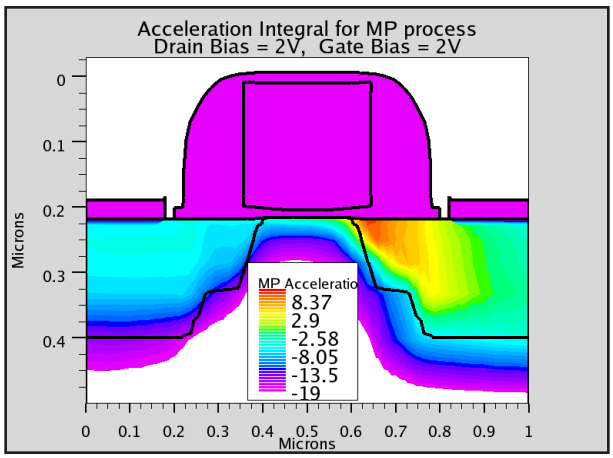

Figure 8. MP Acceleration integral at 2V drain bias (logarithmic scale).

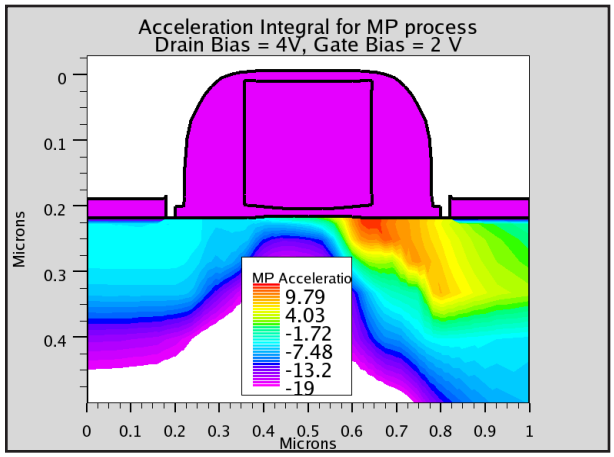

Figure 9. MP Acceleration integral at 4V drain bias (logarithmic scale).

In order to study the MP process in isolation the SP Keldysh cross-section $\sigma^{e}_{sp,0}$ was set to zero and the MP Keldysh cross-section $\sigma^{e}_{mp,0}$ was set to be $1.0 \times 10^{-13}\, cm^2$, with default values for other parameters, including a threshold energy of 1 eV. The default parameters give a value of P_{emi} of approximately 0.036 /second, and so at 100 seconds the time evolution will be essentially complete. The saturated dangling bond density N_a^{mp} was set to $1 \times 10^{13}\text{cm}^{-2}$. With a gate bias of 2 V, a BTE solution was obtained at a drain voltage of 2 V and also at a drain Voltage of 4 V. The MP Acceleration integral is shown in Figures 8 and 9 for these two bias points. There is less difference between the two cases than for the SP process, due to the lower threshold energy. From Figure 6, it is shown that the distribution functions are very similar up to about 1.5 eV, and consequently give similar contributions to the MP acceleration integrals in this range. Because of the lower threshold energy and higher value of cross-section the values of the MP acceleration integral are much higher than the SP acceleration integral under the same conditions. High values are required to give a sizeable value of interface charge density, and in Figure 10 it is seen that the maximum of interface charge density is at the same position as the maximum acceleration integral.

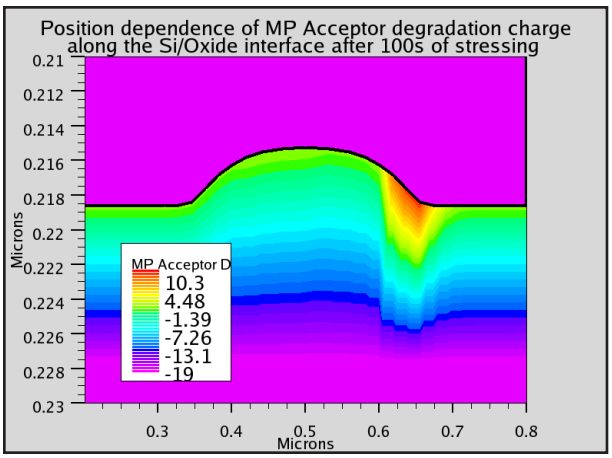

Figure 10. Trapped interface charge density from MP process.

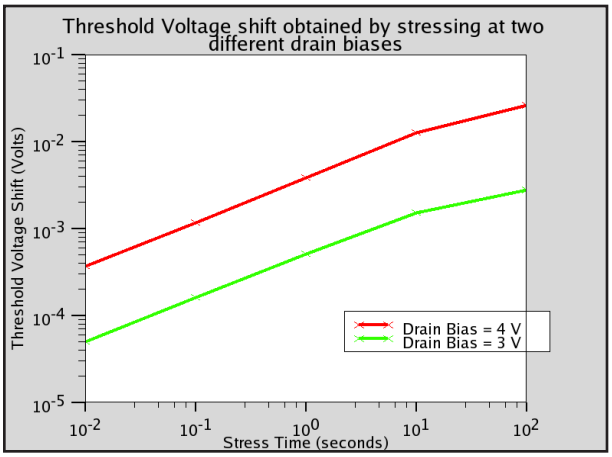
Threshold Voltage shift obtained by stressing at two
different drain biases
Threshold Voltage Shift (Volts)
Stress Time (seconds)
Drain Bias = 4 V
Drain Bias = 3 V

Figure 11. Threshold Voltage shifts due to MP process as a function of stressing time.

The simulation was performed with the same degradation times as before, and for drain biases of 3 V and 4V. The resulting shifts in threshold voltage are shown in Figure 11. At a drain bias of 2 V the shifts were negligible.

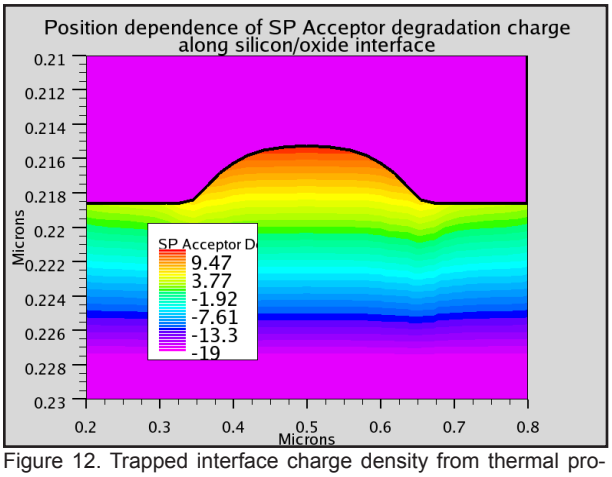

Figure 12. Trapped interface charge density from thermal process.

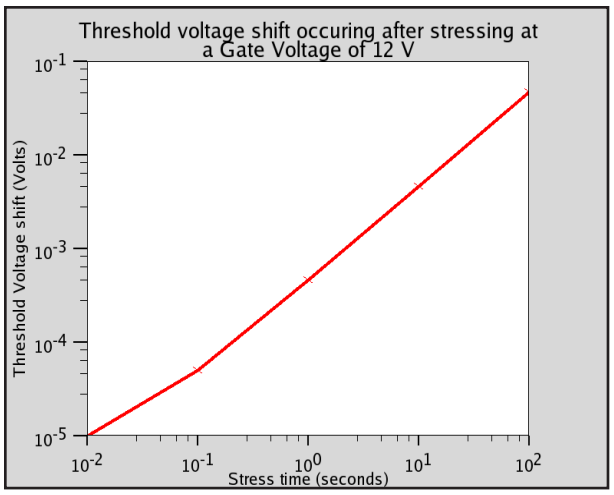
Threshold voltage shift occuring after stressing at
a Gate Voltage of 12 V
Threshold Voltage shift (Volts)
Stress time (seconds)

Figure 13. Threshold Voltage shifts due to field-enhanced thermal process as a function of stressing time.

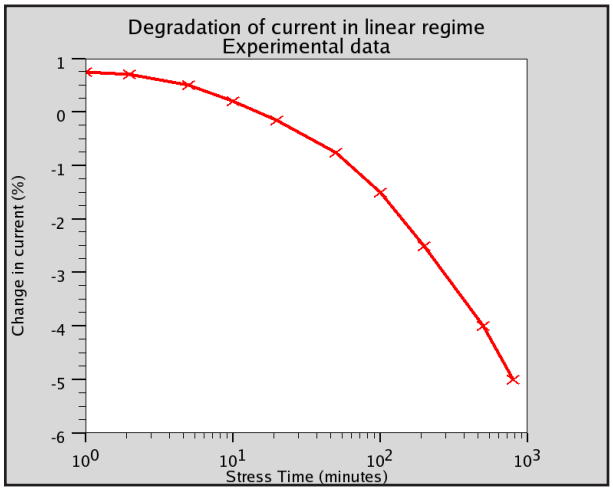

Figure 15. Experimental degradation data (Linear drain current).

The final mechanism to consider is the field-enhanced thermal degradation. The cross-sections $\sigma^{e}_{sp,0}$ and $\sigma^{e}_{mp,0}$ were set to zero, and the rate K_{therm} was changed from its default value of 0 to be $1 \times 10^{12} s^{-1}$. The saturated dangling bond density N^{a}_{sp} was set to $4 \times 10^{12} cm^{-2}$. The gate was biased to 12 V with a drain bias of 0.01 V and the simulation carried out for the degradation lifetimes as above. The interface charge density, shown in Figure 12 after 100 s of stressing, is much more uniform than in the case of either SP or MP process degradation. The threshold voltage shifts typical of this process are shown in Figure 13.

Fitting to Experimental Data

In an actual MOS device all of the three aforementioned degradation mechanisms may be important. In this section results from the model are used to analyze experimental data for a p-channel MOSFET. The device structure is shown in Figure 14 and the stressing biases are gate bias set to -2.1 Volts and drain bias set to -5.5 Volts, with all other contacts grounded. At these biases impact ionization is significant and so degradation by both electrons and holes is important. Impact ionization scattering can be included in the Boltzmann transport solver by specifying BTE.IMPACT on the MATERIAL statement. The main degradation metric used was the change in current in the linear regime, at a fixed gate bias. This shows an enhancement at short stressing time and a decrease at longer simulation time, as shown in Figure 15. One possible interpretation is that some interface acceptor traps are created on a very short time scale with a larger contribution from interface donor traps occurring over a longer stressing timescale.

The device stressing was simulated by using the Boltmann transport equation solver for both electrons and holes with simulation times of 1,2,5,10,20,50,100,200,500 and 800 minutes respectively. The trap densities were set as follows

```
DEGRADATION NTA.SP=0.0 NTA.MP=1.8e13
NTD.SP=1.0e13 NTD.MP=0.0
```

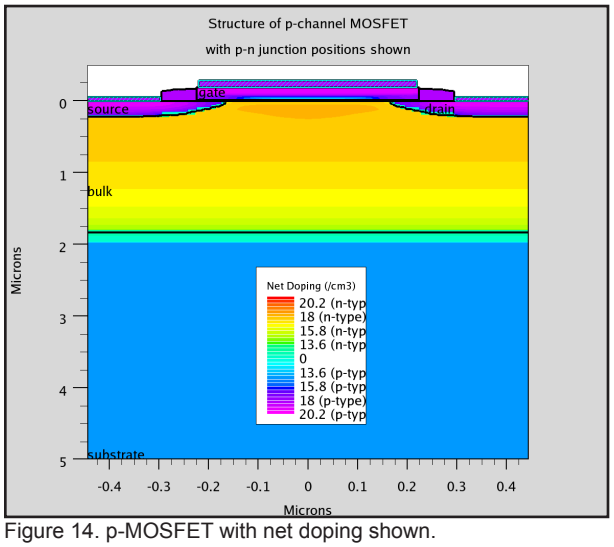

Figure 14. p-MOSFET with net doping shown.

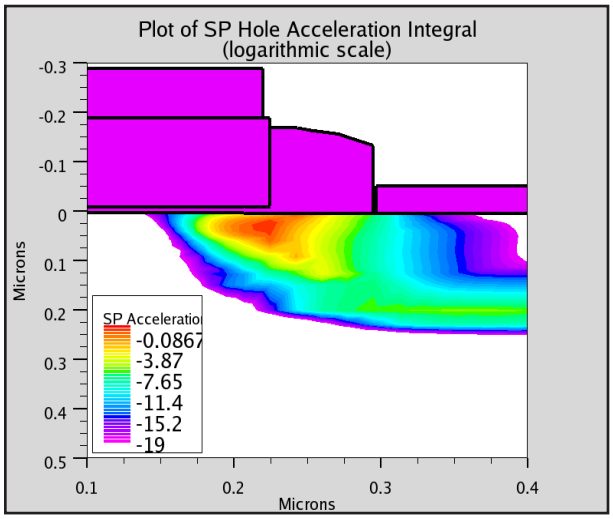

Figure 16. SP process acceleration integral.

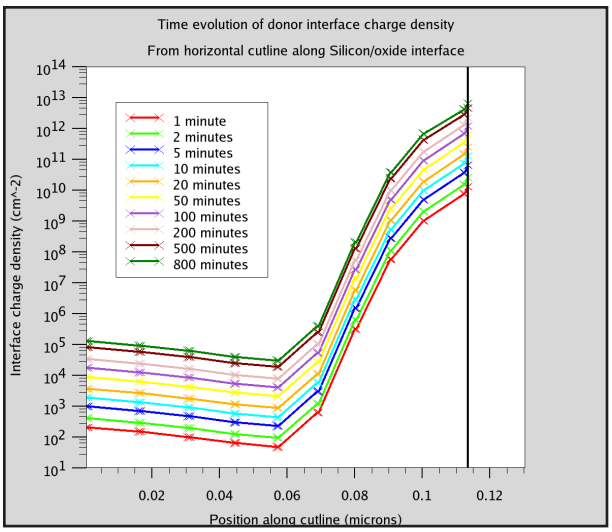

Figure 17. Stress time evolution of donor interface charge.

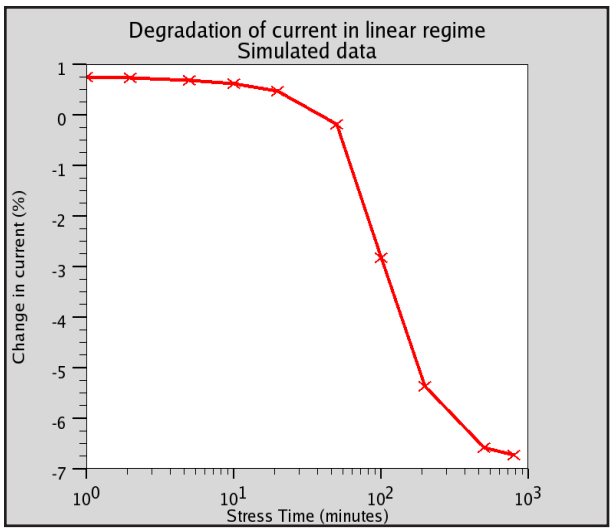

Figure 18. Simulated degradation data (Linear drain current)

and the emission and passivation parameters were set as follows

```
DEGRADATION GF.BARREMI=0.775
GF.BARRPASS=0.725 GF.NUEMI=1.0E12
GF.NUPASS=1.0E12
```

which result in a lifetime associated with the MP processes of approximately 50 seconds in the simulation. Other MP process parameters were

```
ELEC.MP.THRESH=0.5 ELEC.MP.SIGMA=1.0e-
10 ELEC.MP.POWER=3
```

resulting in an MP electron integral having a maximum value of over 10^{13}/s, and a saturated acceptor charge density along a 0.06 microns length of the device. This gives the initial enhancement in the current as the negative interface charge is created, which persists until approximately 10 minutes.

The time evolution of the donor traps depends on $K^h_f(SP)$(**r**) and this quantity is shown in Figure 16. The Keldysh parameters used were

```
HOLE.SP.THRESH=2.3 HOLE.SP.SIGMA=2.0e-
19 HOLE.SP.POWER=4
```

and as can be seen from the figure this produces a maximum value of $K^h_f(SP)$(**r**) of about 15 s^{-1}. The maximum value is away from the interface, and on the interface the maximum value is of the order of 1 s^{-1}, but with a significant part of the interface having values down to $10^{-5}s^{-1}$, which match the maximum timescale of the degradation stressing. Figure 17 shows the evolution with stressing time of the interface charge, along a part of the interface. The positive interface charge generated then reduces the drain current at -5 V, with the current reducing with increased stress time. The percentage change in current is shown as a function of stressing time in Figure 18. This simulation shows good qualitative agreement with experiment.

References

[1] *Atlas User's Manual*, Silvaco, (2014).

[2] C. Guerin, V. Huard and A. Bravaix,' General framework about defect creation at the Si/SiO2 interface', *J.Appl. Phys.*, Vol. 105, (2009), 114513.

[3] I. Starkov,S. Tyaginov, H. Enichlmair, J.Cervenka, C.Jungemann, S. Carniello, J.M.Park, H.Ceric and T.Grasser,'Hot-carrier degradation caused interface state profile - Simulation versus experiment', *J.Vac. Sci. Technol B*, Vol. 29, 01AB09-1/8 (2011).

[4] S.Reggiani,G.Barone,S.Poli,E.Gnani,A.Gnudi,G.Baccarani, M-Y.,Chuang, W.Tian, R.Wise,'TCAD Simulation of Hot-Carrier and Thermal Degradation in STI-LDMOS Transistors',IEEE Trans. Elec. Dev. Vol. 60, No.2 , (2013), pp.691-698.

[5] D.Ventura, A.Gnudi, G.Baccarani, 'A deterministic approach to the solution of the BTE in semiconductors', Rivista del Nuovo Cimento, Vol. 18, No. 6 pp. 1-32, (1995).

Simulations of Deep-Level Transient Spectroscopy for 4H-SiC

1. Introduction

Silicon carbide is expected to be an excellent device material as high voltage and low-loss power devices. Recently, SBD (Schottky Barrier Diode) and MOSFET based on silicon carbide have been realized [1-3], however, those devices have some problems for its reliability and control of the IV characteristics. The problems are related to defects in the bulk and at the interface of insulator/semiconductor. The concentration (~5e12[/cm^3]) of the defects is 2 orders higher than that of silicon [4], and so the defects cause degradation of device characteristics. The investigation of the defect property is important for the improvement of the device performance.

The DLTS (Deep Level Transient Spectroscopy) is one of the method used in measuring material properties such as energy levels and electrons and holes capture cross sections. The device simulator: Atlas can specify an energy level and a capture cross section, and then, can simulate the DLTS signal. So, we can calibrate the defect properties to the DLTS measurement data accurately and the derived defect properties can be applied to the simulations of device characteristics.

In this article, we demonstrate device simulations of the DLTS signal for a SBD structure with the Z1/Z2 center trap of carbon-vacancy in the bulk.

2. DLTS Measurement

The DLTS measurement can be applied to simple device structures like the PN junction device, the Schottky device and the MOS device as shown in the Figure 1 [5].

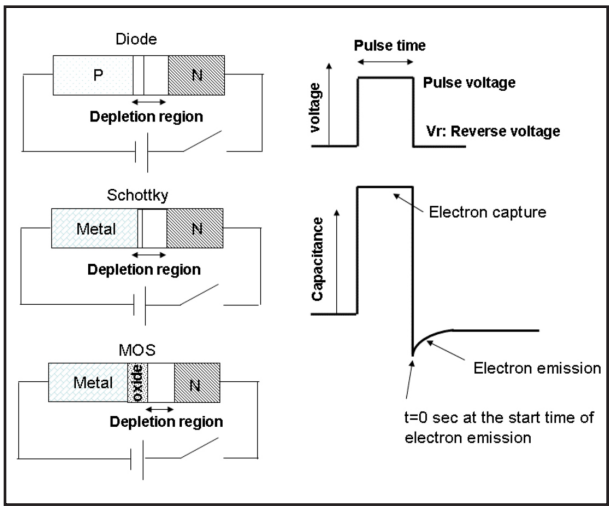

Figure 1. DLTS measurement applied to simple device structures.

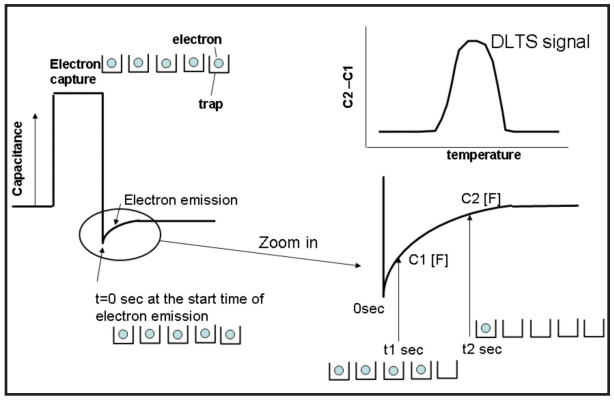

Figure 2. Procedure to obtain the DLTS signal.

The Schottky structure is suitable to the investigation of the traps in the bulk semiconductor with an uniform doping. The DLTS signal can be obtained by the following procedure.

1) A reverse voltage is applied to a device creating a depletion region. As a result nearly all traps have emitted an electron.
2) 0V is then applied to this device for a certain time such that nearly all traps have captured an electron. This time is called “pulse time”.
3) Finally the device is biased back in reverse mode in a very short time and this reverse bias is maintained. As shown in Figure 2, electron emission is time dependent and the relaxation process changes the capacitance. By measuring the difference of capacitance between t1 and t2 you can measure temperature dependence of the capacitance difference. That temperature dependence is called “DLTS” signal.

3.DLTS Simulation of a Schottky Structure with a Single Trap in the Bulk

The DLTS simulation needs to do transient simulation and AC small signal analysis simultaneously. And the capacitance difference depends on the trap concentration. If the doping of N- is 1e15 level and its trap concentration is less than the order of 1e13 [1/cm^3], the capacitance difference becomes less than the order of 1e-19 [F] and it is very small. This simulation needs to calculate the capacitance considerably accurately.

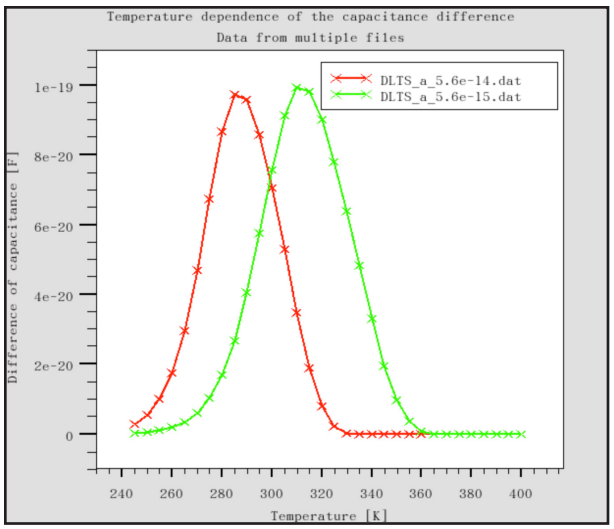

Figure 3. Two DLTS signals.
(Red line: sign=5.6e-14[cm^2], Green line: sign=5.6e-15 [cm^2])

Figure 3 shows two results of the DLTS simulation. The simulation condition is described as below.

- Structure/Electrode as shown in Figure 4
  - 4H-SiC substrate: Depth: 12um,

    Dopant: N- type, concentration: 5e14 [/cm^3], N+ type concentration: 1e20 [/cm^3], by distance of 2um from cathode
  - Anode: Schottky barrier height: 1.2 eV
  - Cathode: Ohmic
- Bulk Trap condition
  - Z1/Z2 center trap due to the carbon vacancy
  - energy level (Ec-Et):0.66 eV
  - density: 1e13 [/cm^3]
  - capture cross section (sign): 5.6e-14 [cm^2] and 5.6e-15 [cm^2]
  - degeneracy: 1
- Pulse condition
  - pulse voltage: 0V, reverse voltage: -8V
  - pulse time: 10ms
  - t1: 10ms
  - t2: 210ms
- AC small signal analysis
  - frequency: 1e5 Hz

Figure 4 shows the structure used for those simulations. It is formed by 4H-SiC substrate of the depth: 12 um with N-type impurity of 5e14 [/cm^3]. It has an anode electrode with schottky contact on the top, and a cathode electrode with ohmic contact on the bottom. The region of 2 um with N-type doping of 1e20 [1/cm^3] is put on the bottom. Then, The bulk trap condition is assumed to be the Z1/Z2 center trap due to the carbon vacancy. The energy level, the concentration and the degeneracy of the trap are 0.66eV, 1e13 [1/cm^3] and 1, respectively.

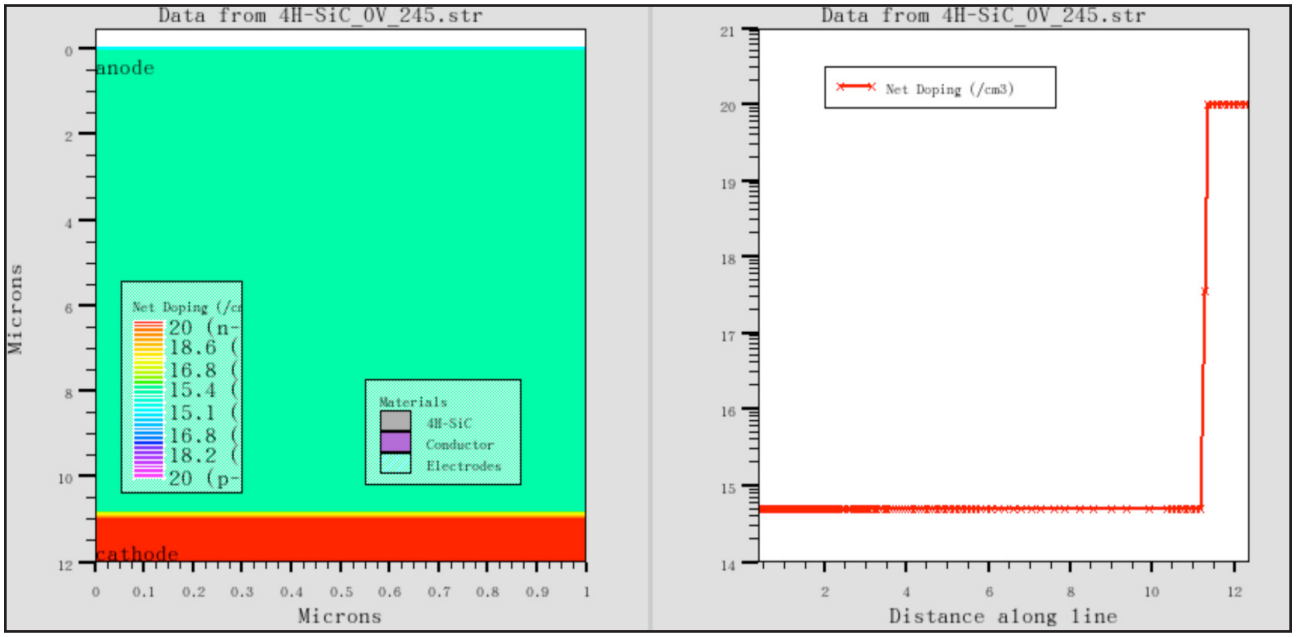

Figure 4. 2D structure of 4H-SiC substrate in right side and 1D doping profile in the left side.

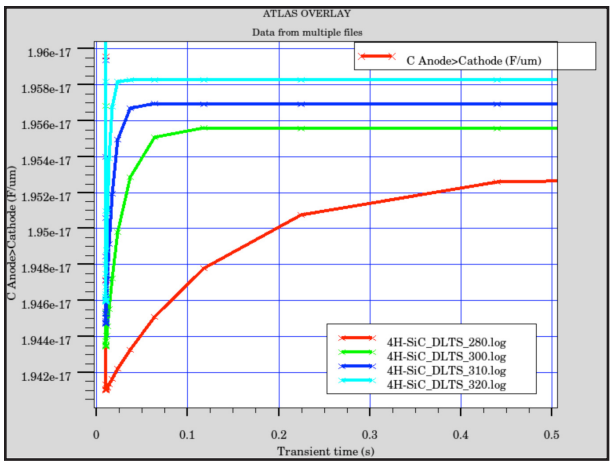

Figure 5. Transient simulations of capacitance (sign=5.6e-14 [cm^2]).

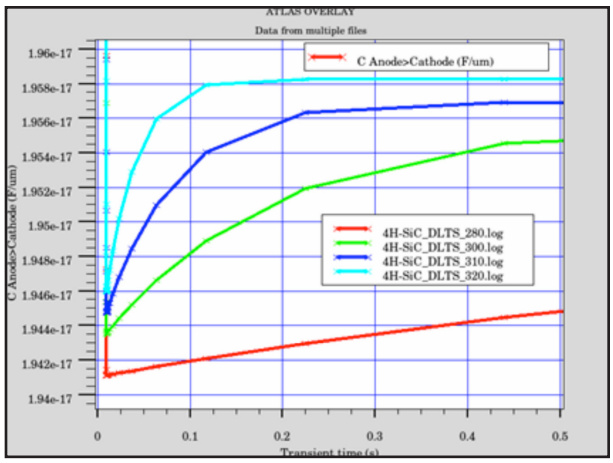

Figure 6. Transient simulations of capacitance (sign=5.6e-15 [cm^2]).

The two DLTS signals correspond to the difference of the capture cross sections. The left and right signals were calculated with sign=5.6e-14 [cm^2] and 5.6e-15 [cm^2], respectively. You can find that larger capture cross section makes lower temperature's peak position, because the relaxation speed of larger capture cross section becomes faster at a same temperature. A DLTS signal of Figure 3 was obtained by 32 transient simulations including the AC analysis, which were calculated with different temperatures by 5 degrees. Figures 5 and 6 shows 4 transient simulations of the electron emitting process in the temperatures: 280, 300, 310, and 320K. You can see that higher temperature makes shorter relaxation time for the electron emitting process from traps.

4. Summary

We have demonstrated that the DLTS (Deep Level Transient Spectroscopy) signal can be simulated by the device simulator: Atlas. The DLTS simulation needs the analysis of the very small capacitance difference and Atlas has the function to carry out the transient simulation and the AC small signal analysis simultaneously and accurately.

References

[1] T. Sakaguchi et al., Tu-P-59, p.171, ICSCRM 2013

[2] M. Okamoto et al., Mo-1A-4, p.10, ICSCRM 2013

[3] F. Devynck, Thesis, Figure 1.4, p. 8, 2008

[4] T. Hatakeyama et al., Materials Science Forum , pp.477-480, Vols, 740-742, 2013

[5] K. Matsuda, Horiba Technical Reports, "Semiconductor Impurities and Defects Evaluation by ICTS and DLTS", pp.15-26, No.2, January, 1991

Hints, Tips and Solutions

Q: Using TonyPlot, can I achieve publication quality plots?

A: Yes, TonyPlot has many various display and preference settings that users can adjust, transforming their simulation data into a high quality plot for use in publications.

Example: SiC Example #10 – SiC MOSFET Breakdown Simulations

Silvaco includes examples with every software package. One example, sicex10, simulates the effect of both layout and trench geometries on breakdown voltage for a 3D SiC MOSFET. In short, it is found that a rounded layout corner as well as a sloped trench sidewall increases the MOSFET breakdown voltage. The resulting output, plotted in TonyPlot, is shown in Figure 1.

While this plot is perfectly acceptable for display and analysis of simulation results, a user may want to convert the plot for use in a publication submission. TonyPlot has numerous options that can be modified to increase plot clarity, meeting any given journal's publication standards.

By performing the simple steps detailed in this tip, Figure 2 is obtained. In this example a black and white figure format is chosen, as this is often the preferred format of many peer-reviewed journals and transactions. However, these 15 modifications are just a few examples of the numerous options available in TonyPlot. For more details, consult the TonyPlot Manual, or contact your local Silvaco sales and support office for more information.

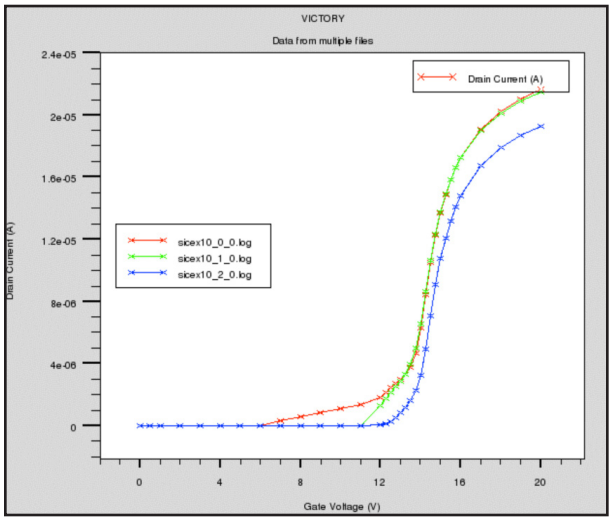

Figure 1. Plot of breakdown voltage simulations from sicex10 using default TonyPlot settings.

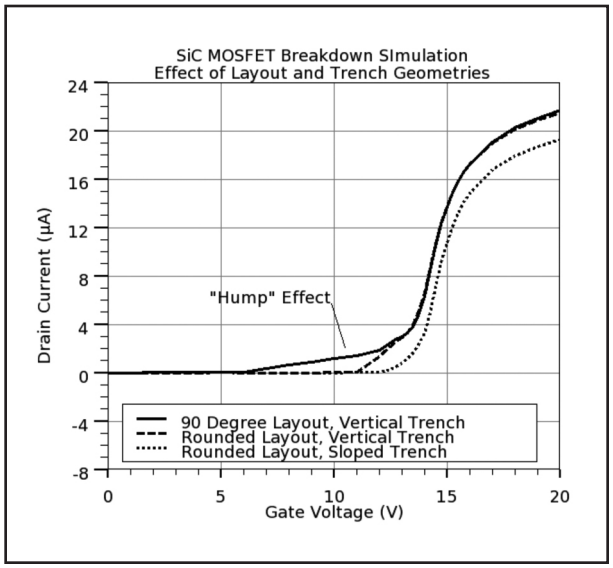

Figure 2. Plot of breakdown voltage simulations from sicex10. Modifying the TonyPlot settings, as described in this document, converts Figure 1 into a publication-worthy figure.

In this example, the plot is modified in TonyPlot in the following ways:

1. **Modify Drain Current units from A to μA** – Using Plot >> Display >> Functions add "Drain Current*1e6" to Graph Func 1, click ok. Then, in the display window, deselect drain current from the list of Y Quantities and select Function 1. This will convert the displayed drain current magnitude from Amps to micro-Amps.
2. **Modify Y-Axis Label** – Using Plot >> Annotations, type a Y-Axis label "Drain Current (<mu>A)" and TonyPlot will convert the bracketed text <mu> to the Greek symbol μ.
3. **Adjust X/Y Min, Max, Divisions and Ticks to Fit Datasets:** Using Plot >> Annotations, the X and Y axis properties are specified.
4. **Add Main and Subtitles to the Plot: Using Plot** >> Annotations, the title "SiC MOSFET Breakdown Simulation" and the subtitle "Effect of Layout and Trench Geometries" are added.
5. **Turn Off Line Markers:** Using Plot >> Display, the plot markers button can be deselected.
6. **Change All Line Colors to Black:** Using Preferences >> Sequence Colors, the 1st, 2nd and 3rd sequence colors are all changed to black.

7. **Change Line Types to Differentiate the Curves:** Using Preferences >> Sequence Lines, adjust the 1st, 2nd and 3rd sequence lines to different line types (solid, dashed, dotted, etc.) and set Preferences >> Overlay Options >> Display Option to "Color/Mark."
8. **Increase Line Thickness:** Using Preferences >> Drawing Options >> Graphs, increase line widths.
9. **Modify Plot Fonts:** Using Preferences >> Drawing Options, the small, medium and large Font style and size can be changed.
10. **Increase Plot Margins:** Using Preferences >> Plot Options >> Plot Margins, the left, right, top and bottom margins can be adjusted.
11. **Change Plot Window Colors:** Using Preferences >> General Colors >> Window, the border color can be changed to white.
12. **Add Gridlines and Modify Gridline Color:** Using Plot >> Annotation, the "show gridlines" toggle button is selected. Using Preferences >> General Colors >> Grid, the grid color can be changed as well.
13. **Adjust Which Keys are Shown and their Location:** Using Preferences >> Key Options, the "Graphs" key can be turned off, and the location and transparency of the "Levels" key can be changed.
14. **Modify Level Names:** Using Plots >> Level Names, the name of the 3 line traces can be changed. Additionally, the marker toggle button can be deselected to remove markers from the key.
15. **Add Labels for Emphasis:** Using Plot >> Labels, text with arrows can be overlaid on the plot to add emphasis.

Users can also utilize the File >> Save Set Files, to save many of the settings for use in other plots.

Call for Questions

If you have hints, tips, solutions or questions to contribute, please contact our Applications and Support Department

Phone: +1 (408) 567-1000 Fax: +1 (408) 496-6080

e-mail: support@silvaco.com

Hints, Tips and Solutions Archive

Check out our Web Page to see more details of this example plus an archive of previous Hints, Tips, and Solutions

www.silvaco.com

Hints, Tips and Solutions

Q. How can I calculate light extraction efficiency in an OLED or LED with pure optical simulation?

A. Calculation of light extraction efficiency or optical output coupling efficiency is often needed in simulating a light emitting device (LED) such as an organic LED (OLED). It is best to perform these calculations without running electrical simulation in the device, as parameters for new materials are hard to obtain and generally unnecessary in calculating light extraction efficiency. Moreover, a pure optical simulation will save simulation time and avoid any potential un-convergence in the electrical simulation.

The above-mentioned simulation is able to be carried out in Atlas. In the simulation, complete channels of power dissipation from an electric dipole (e.g., an exciton) are analyzed, and the light propagation and distribution is determined by a matrix method. (Ref. [1] contains physics details.) The only required material parameter for the simulation is the complex refractive index at a given wavelength or within a wavelength range of interest. Since the light extraction calculation in Atlas can only be done on top of the device, the device has to be created upside down if the light is collected from the substrate. A scheme of a flipped bi-layer OLED (Figure 1) consisting of a Ag layer, a Alq3 layer, a hole transport layer (HTL), an ITO Layer, and a glass substrate. The device has been flipped up and down with the substrate on the top. A dipole located at the HTL and Alq3 interface, denoted by the yellow dot in Figure 1, will be analyzed as the light-emitting source. Note that no electrode specification is needed here.

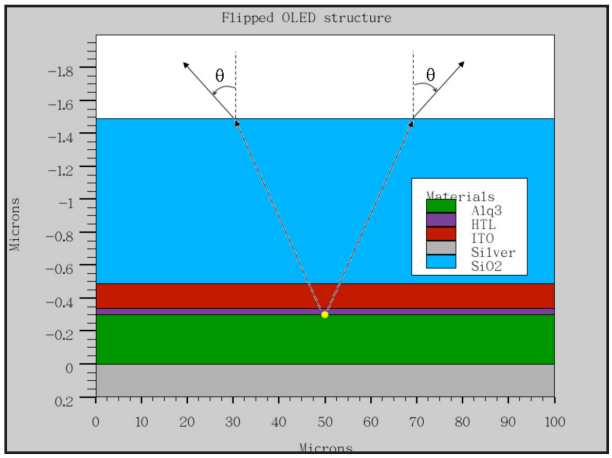

Figure 1. Scheme of a flipped bi-layer OLED.

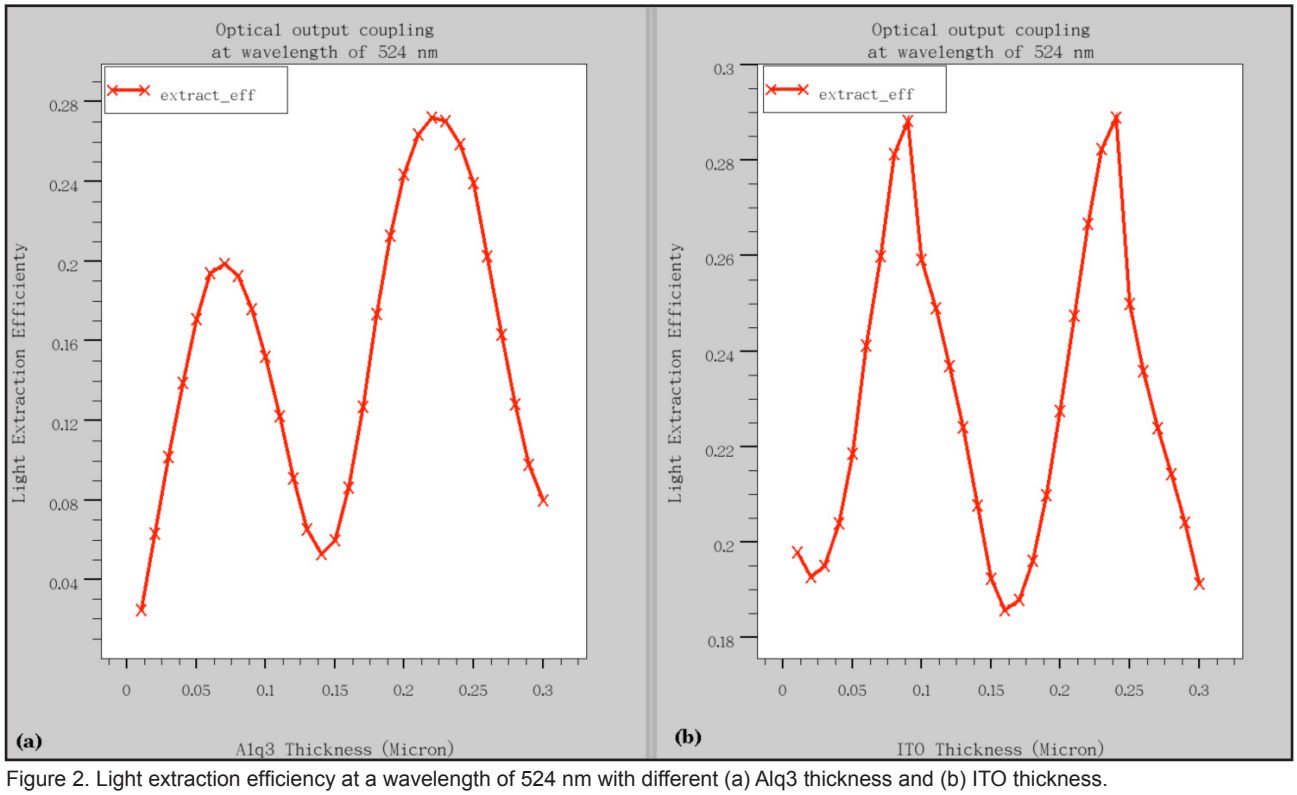

Figure 2. Light extraction efficiency at a wavelength of 524 nm with different (a) Alq3 thickness and (b) ITO thickness.

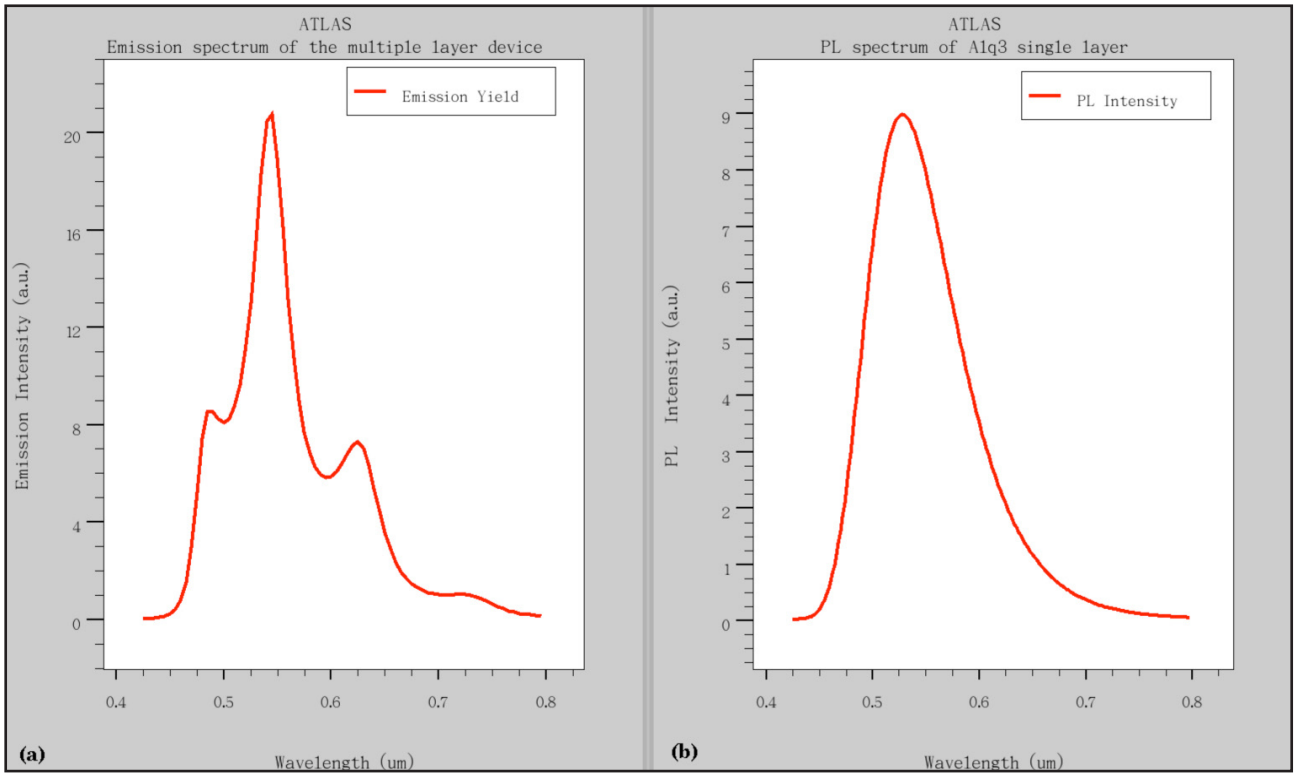

Figure 3. (a) Simulated emission intensity spectrum of the device, and (b) user-specified PL intensity spectrum of the Alq3 single layer material.

After specifying the refractive index of each layer, the optical simulation can be run simply using SAVE statements without any SOLVE statement, as follows,

```
save x=50 y=-$t_alq3 l.wave=0.524
       n.surf=1 d.orient=1
angle.out=90 dos.maxn=20 opdos=total.dat
```

where x and y defines the location of the dipole, l.wave specifies the wavelength in micron, n.surf specifies the real part of the surface refractive index. d.orient=1 means a randomly oriented dipole is considered. angle.out specifies an angle with respect to the vertical axis, as indicated in Figure 1 by θ, the output light power will then be calculated from –θ to θ. dos.maxn specifies the upper limit of the integral over the normalized wavevector parallel to the x axis. By setting dos.maxn with a value much larger than 1, total emission power from the dipole will be calculated. The simulation result is saved to the file total.dat.

In order to calculate the power emitted out of the device from the same dipole, we have to restart Atlas, create the structure again, and use another SAVE statement but with dos.maxn=1:

```
save x=50 y=-$t_alq3 l.wave=0.524
       n.surf=1 d.orient=1
angle.out=90 dos.maxn=1 opdos=photon.dat
```

In this case the integral over the parallel normalized wavevector is limited within [0, 1], which means the vertical wavevector is always real. Thus the light will propagate non-evanescently out of the device. The simulation result is saved to the file photon.dat.

With the file total.dat and photon.dat, we now can calculate the light extraction efficiency using several EXTRACT statements:

```
extract init inf="photon.dat"
extract name="air_emis"
max(curve(elect."Wavelength",
   probe."DOS (Para)"*2/3+probe."DOS
   (Perp)"/3))
extract init inf="total.dat"
extract name="total_emis"
max(curve(elect."Wavelength",
   probe."DOS (Para)"*2/3+probe."DOS
   (Perp)"/3))
extract name="light_extract_eff" $air_
emis/$total_emis
```

The emission power coming out of the device and the total emission power is extracted and saved to the variable air_emis and total_emis, respectively. The ratio of these two parameters is the light extraction efficiency which is saved to the variable light_extract_eff. Figure 2 shows the light extraction efficiency with different (a) Alq3 thickness and (b) ITO thickness after parameter sweeping simulations.

Given the photoluminescence (PL) spectrum of the active material, the emission spectrum from the device can also be obtained by the same optical simulation. The following example demonstrates such a simulation in the same device given in Figure 1.

```
save x=50 y=-$t_alq3 n.surf=1 d.orient=1
  lmin=0.425 lmax=0.795 t.init=0.005
  t.min=0.005
  angle.out=1 dos.maxn=20 opdos=ignore
  yield=emis_spec.dat user.spect=alq3_
  spect.spec
```

In the above SAVE statement, lmin and lmax defines the wavelength range, t.init and t.min specifies the initial and minimum wavelength step in the simulation respectively. The output angle is set to 1° here, therefore the output power will be calculated within 2° around the y axis. User-defined PL spectrum of Alq3 is given in the file alq3_spect.spec and the simulated emission spectrum is saved in emis_spec.dat. A string "ignore" is assigned to opdos, which means no data will be saved for opdos. The resultant emission spectrum is shown in Figure 3(a). User-defined PL spectrum is plotted in Figure 3(b) for comparison. A direct application of such a simulation is that the electroluminescence (EL) spectrum can be obtained in combination with an electrical simulation. In that case, the actual dipole density at a given position will be used to calculate the emission power.

One should bear in mind that due to the functional limit of the matrix method, the pure optical simulation is restricted to one dimension (1D) only. Namely, no refractive index variation along the x axis is allowed in the simulation.

Reference

[1] R. R. Chance, A. Prock, and R. Silbey, "Molecular fluorescence and energy transfer near interfaces", Adv. Chem. Phys., Vol. 37, pp. 1-65 (1978).

Call for Questions

If you have hints, tips, solutions or questions to contribute, please contact our Applications and Support Department
Phone: +1 (408) 567-1000 Fax: +1 (408) 496-6080
e-mail: support@silvaco.com

Hints, Tips and Solutions Archive

Check out our Web Page to see more details of this example plus an archive of previous Hints, Tips, and Solutions

www.silvaco.com

USA Headquarters:

Silvaco, Inc.
4701 Patrick Henry Drive, Bldg. 2
Santa Clara, CA 95054 USA

Phone: 408-567-1000
Fax: 408-496-6080

sales@silvaco.com
www.silvaco.com

Worldwide Offices:

Silvaco Japan
jpsales@silvaco.com

Silvaco Korea
krsales@silvaco.com

Silvaco Taiwan
twsales@silvaco.com

Silvaco Singapore
sgsales@silvaco.com

Silvaco Europe
eusales@silvaco.com

SILVACO